The Journal of Experimental Biology 212, 1413-1420
Published by The Company of Biologists 2009
doi:10.1242/jeb.020636

The material properties of acellular bone in a teleost fish

Jaquan M. Horton* and Adam P. Summers

Department of Ecology and Evolutionary Biology, University of California Irvine, CA 92697, USA and Friday Harbor Laboratories, University of Washington, Friday Harbor, WA 98250, USA

*Author for correspondence (e-mail: jhorton@uci.edu)

Accepted 11 February 2009

SUMMARY

Several lineages of teleost fishes have independently derived skeletons composed solely of acellular bone, a tissue without obvious advantages over bone that has osteocytes in the matrix. There is no consensus for the functional role of acellular bone, as factors such as salinity, activity level and gross morphology have been shown to be poor predictors of acellularity. We used a three-point bending method to test the hypothesis that the material stiffness (elastic modulus) of acellular bone is higher than that of cellular bone, which could be evidence that material properties were a selective pressure in the evolution of this unusual skeletal material. The acellular ribs of *Myoxocephalus polyacanthocephalus* are curved, hollow beams that decrease in size both distally and posteriorly along the rib series. First and second moments of area decreased distally and caudally in all individuals. Young's modulus (*E*) ranged from 3.67 to 8.40 GPa, with a mean of 6.48 GPa. The flexural stiffness (*EI*) differed significantly between ribs, and the hollow cylinder morphology increased the flexural stiffness by 12.0% over a solid, circular cross-section rod with the same area. Contrary to our expectations, acellular bone is not stiffer by virtue of fewer lacunae but instead falls at the very low end of the range of stiffness seen in cellular bone. There remains the possibility that other properties (e.g. fatigue resistance, toughness) are higher in acellular bone.

Key words: acellular bone, material properties, Young's modulus, stiffness, ribs

INTRODUCTION

Vertebrate bone can be either cellular or acellular (Kölliker, 1859; Moss, 1960), a distinction based on whether osteocytes are embedded within the mineralized matrix (Moss, 1960). The presence of osteocytes creates a morphologically distinctive skeletal material with an extensive interconnected network of microscopic canals (canaliculi) associated with cell lacunae (Gray, 1941; Moss, 1961; Mjor, 1962; Wassermann and Yaeger, 1965; Cowin, 2007). Dendritic processes radiate from the osteocytes and project into these canals allowing for direct communication between the adjacent osteocytes and the external environment *via* gap junctions (Aarden et al., 1994; Donahue, 2000; Kusuzaki et al., 2000). Within this network, osteocytes function as mechanoreceptors that facilitate metabolic activities such as calcium hydrolysis, bone modeling and bone remodeling (Lanyon, 1993; Burger and Klein-Nulend, 1999; Burr et al., 2002).

Osteocytes are a significant presence in cellular bone, as their numbers range from 31,000 to 93,000 cells mm^{-3} for mammalian species (Mullender et al., 1996). Although acellular bone lacks osteocytes within the bone matrix, it is still capable of recruiting periosteal osteocytes to regulate bone modeling and remodeling (Takagi and Yamada, 1992; Kranenbarg et al., 2005b), and to offset acalcemic conditions in both the environment and diet (Takagi and Yamada, 1993). However, when a calcium deficiency exists in both water and diet, callus formation during fracture repair in acellular bone is poor compared with that in cellular bone (Moss, 1962). Nevertheless, acellular bone is able to adapt to changes in loading regime by modeling and remodeling to decrease the strain resulting from an applied load.

Acellular bone is a plesiomorphic character in vertebrates found in both primitive craniates and vertebrate lineages (Ørvig, 1965; Ørvig, 1989). The dermal bones of several extinct jawless craniates (notably the Heterostraci, Anaspida and Thelodonti) were of aspidin, a type of acellular bone. However, the exoskeletal head shields of the Osteostraci (jawless vertebrates) were covered with cellular bone (Hanken and Hall, 1993), as were components of the feeding apparatus of Conodonts, the earliest known vertebrates (Sansom et al., 1992), and elasmoid fish scales (Meunier et al., 2003; Meunier et al., 2004). However, teleost fishes are the only vertebrates with a skeleton composed solely of acellular bone (Moss, 1961). Mapping acellular bone on the teleost phylogeny suggests an increasing trend toward acellularity, with the superorder Percomorpha containing a little more than 85% of known acellular bony fishes (Kranenbarg et al., 2005a). The multiple origins of acellularity within teleosts indicate a possible selective advantage of this type of bone, yet there is no consensus for the functional role of acellular bone, as the factors that have been investigated such as environment, activity level and gross morphology do not predict the presence of acellularity (Moss and Freilich, 1963; Moss, 1965). Therefore, the adaptive significance or selective pressures that lead to the repeated evolution of acellular bone in the teleosts remain unclear.

A functionally important mechanical property of bones is stiffness, both in the whole element sense and in the material sense. For example, the long bones of vertebrates must be stiff enough to provide the necessary support to act as efficient levers (Currey, 2002). Moreover, the mechanical properties of bones are influenced by several hierarchical levels of organization, including composition and microstructure (Fratzl and Weinkamer, 2007). One factor that affects stiffness is porosity at the microscale (1–100 μm), as an increase in bone porosity will cause a substantial reduction in stiffness. Schaffler and Burr (Schaffler and Burr, 1988) derived a formula from

experimentation that suggests that bone with normal mammalian cellularity will be about 73% as strong as bone without the cell spaces. This raises the possibility that the adaptive significance and selective pressures that lead to the repeated evolution of acellular skeletons in teleost fishes is an increase in stiffness relative to cellular bone.

The aim of this study was to measure flexural stiffness and second moment of area (I) in order to determine the modulus of elasticity (Young's modulus, E) in an exemplar acellular fish bone to: (1) test whether acellular bone is stiffer than literature values for cellular bone in other fish and terrestrial vertebrates; (2) determine the variation in stiffness across the rib series from the anterior to the posterior direction; (3) assess variation in the stiffness of ribs from proximal to distal; and (4) partition variation in the flexural stiffness of the ribs into a structural component (I) and a material component (E).

MATERIALS AND METHODS

Specimens

The great sculpin, *Myoxocephalus polyacanthocephalus* (Pallas 1814), is a demersal, amphidromous fish with an acellular bony skeleton. Six *M. polyacanthocephalus* (285–375 mm total length) were collected by seining at Jackson's Beach, Friday Harbor, WA, USA. Morphometric measurements were taken after fish had been killed with an overdose of MS-222 (tricaine methanesulfonate). All animal experimentation was performed in accordance with the University of Washington Animal Care and Use Committee rules.

Rib dissection

Ribs were dissected from the left side of fresh frozen fish. Excess connective tissue was removed under a dissection microscope with jeweler's forceps. Ribs were measured, and marked with a permanent felt-tip marker at three positions along their length (25%, 50% and 75% of total length) – proximally to distally, and stored in teleost Ringer solution at 6°C for no more than 48 h before tests were performed. The first 12 ribs of *M. polyacanthocephalus* were used for this study; ribs 13 and 14 are reduced and extremely fragile and were difficult to remove without fracturing.

Material testing and area analysis

We used a three-point bending test to measure flexural stiffness of fish ribs. Tests were performed on a custom-made fixture mounted in a Synergie 100 test system (MTS, Eden Prairie, MN, USA) with either a 500 N load cell or a 50 N load cell depending on rib size. Ribs were supported by two load points with a 1 cm span and centrally loaded with a minimal force (approximately 0.005 N) to secure the bone in place, and to ensure zero rotation along the long axis. The slight natural curvature of the rib bones ensured that each specimen and location were tested in the same anatomical orientation: the medial surface of the rib was depressed by the indenter, and the two supports were in contact with the lateral surface. We then loaded the rib four times at each location (25%, 50% and 75%), in a random order, to a maximum deflection of 0.3 mm at a test speed of 0.1 mm s^{-1}; data were acquired at 120 Hz. Bone has a very small viscous component, so our choice of indenting speed (strain rate) should not affect the measured flexural stiffness. The deflection distance was chosen to minimize the possibility of micro-crack formation; and analysis of the multiple tests at each location did not show any trend toward decreasing stiffness. Some ribs had callused areas but these were well away from the region we tested.

After testing a rib we manually sectioned the bone (0.5–1.0 mm thick) from each of the tested positions using a microtome blade. We then took digital images of the rib cross-section at the point of load contact using a Zeiss dissecting scope (Stemi 2000-C, Jena, Germany) with a top-mounted Spot Insight color camera (IN-320, Sterling Heights, MI, USA). Photographs were transferred to a Macintosh computer using the Spot (v. 3.3.2) software program in a jpeg format. Cross-sectional area (CSA) was measured from the ribs of seven individuals, whereas six were used for material testing. Analysis of photographs and raw output data from material testing was performed using a customized MatLab (v. 7.0) script that calculated the second moment of area with respect to a neutral axis through the center of area parallel to the major axis of the ellipse that best fitted the outline of the cross-section. The rib was tested with the medial surface up, so this neutral axis would be perpendicular to both the long axis of the rib and the direction of deflection. Cross-sectional images were scaled, and both first (geometric) and second moments of area about the neutral axis (NA) were quantified. The script then used the equation:

$$y_{\max} = \frac{\mathbf{F} l^3}{48 E I_{\mathrm{NA}}}, \quad (1)$$

where $y_{\max}$ is the distance the bone was deflected, $\mathbf{F}$ is the force required to deflect the bone to the point $y_{\max}$, and l is the span length. The formula was used for calculating a beam point-loaded at the midpoint of its length. The equation above (Eqn 1) was derived to find the Young's modulus, or material stiffness (E).

Of substantial concern is the determination of E from a beam equation with assumptions that we violated in some way. The most pressing of these is the assumption that the deformations are caused solely by bending rather than shear, which is certainly true for very long thin beams. The literature for prismatic beams of bone indicates that if the ratio of supported length to depth is less than 15:1 then shear plays a substantial role and the modulus will potentially be substantially underestimated (Spatz et al., 1996). Our ratios ranged from 7.5 to 36, with many samples below the cutoff for solid beams. Because there is not even an empirical formula for hollow cylindrical structures we assessed the effect of aspect ratio on stiffness with a regression. There was no relationship between the two variables, and a breakpoint analysis did not show the expected decline in stiffness as the ratio decreased. We attribute this to the hollow cross-section of the beam. The beam equation also assumes a constant cross-section. Though there was a distinct taper to the ribs we chose a very short span so as to minimize the difference between cross-section at the two end supports and we measured first and second moments of area at the indenter. The gross appearance of the ribs is that of a monotonically tapering beam, so we would not expect more than a 10% difference in CSA from one end of the tested section to the other. The very slight curvature of the rib amounted to a ratio of radius of curvature to depth of more than 8, so we can ignore the curvature (Young and Budynas, 2002).

We quantified the contribution of the hollow cylinder morphology to the flexural stiffness of the rib by calculating the ratio of the measured I_{NA} of a rib to that of a solid cylinder with the same first moment of area as the rib section (I_{t}):

$$I_{\mathrm{t}} = \frac{A_{\mathrm{R}}^2}{4\pi}, \quad (2)$$

where A_{R} is the area of the rib cross-section.

Compositional analysis

After material testing, whole hydrated ribs (including segments used for cross-sectional photos) were weighed, and lyophilized for 30 h.

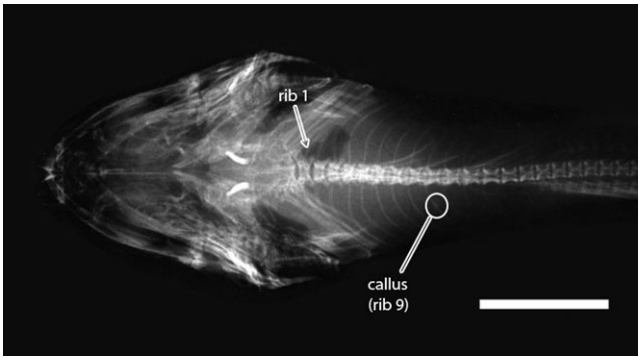

Fig. 1. Dorsal radiograph image of an adult *Myoxocephalus polyacanthocephalus* showing skeletal morphology and the relative position of the dorsal ribs along the body. Note: the ribs project in a posterior–lateral direction and provide no lateral protection of the visceral cavity. Also there is a callus located on the midpoint of rib nine of the left side of the fish. Scale bar, 4 cm.

Dry mass (organic plus mineral material) was recorded for the samples before ribs were placed in a 500°C furnace for 24 h to remove the organic content from the dry mass. The remaining ash content was weighed immediately upon removal from the furnace, to avoid possible water gains from room humidity. Water content was calculated by subtracting the dry mass from the original bone mass, whereas the mineral content is expressed as mass of ash divided by the dry mass.

Statistical analysis

Data were analyzed in SAS (v. 11.0, SAS Windows student version; SAS Institute, Cary, NC, USA). An analysis of covariance (ANCOVA) was used to determine intraspecific differences between CSA, second moment of area (I) and stiffness (E), both along the length of the body (i.e. the rib series) and along a single rib (comparing 25%, 50% and 75% locales), as well as interspecific differences. The use of an ANCOVA allowed for the exclusion of any effects associated with fish length, the covariate. SAS was also used to determine whether percentage mineral content differed between ribs within a fish, and between individuals at a given rib number. All data points referring to a mean value are the combined values from the 25%, 50% and 75% locales for a given rib. Data from multiple tests were pooled for statistical analysis at the same location and rib.

RESULTS

Rib morphology and material properties

Radiograph images from dorsal and ventral viewpoints reveal the relative position of the ventral, or pleural, ribs of *M. polyacanthocephalus* (Fig. 1). Ribs project in a lateral–posterior direction and are positioned within the dorsal portion of the hypaxial musculature; they do not surround the visceral cavity. The length of the ribs ranged from 461 to 312 mm. All ribs were curved, hollow structures that decreased in length posteriorly and in CSA distally. The central cavity varied in width and exhibited great morphological diversity (Fig. 2). The hollow was most prominent in the first six ribs.

The geometric CSA of the ribs decreased significantly from the first to the twelfth rib for all individuals (quadratic regression; R^2=0.87; P<0.001; Fig. 3). Both the linear term ($F_{1,47}$=163.23; P<0.01) and the quadratic term ($F_{1,47}$=25.11; P<0.001) were significant. The quadratic regression best fits the data due to the difference in mean CSA between the first and second rib, which was roughly 40%, and the relatively minor difference in mean CSA between subsequent ribs of approximately 10% (Fig. 3). The absolute maximum CSA was 1.25 mm^2 at the first rib and 0.21 mm^2 at the twelfth rib. Although individuals differed significantly (P<0.001), raw data from each individual exhibited the same trend shown in Fig. 3.

The positional effects of geometric cross-section were measured along the length of the rib at three locations. Mean CSA at each locale decreased significantly from the proximal to the distal end along each rib for all individuals (R^2=0.95; $F_{2,10}$=25.11, P<0.001; Fig. 4A). Accordingly, the proximal (25%), midpoint (50%) and distal (75%) positions differed significantly (P<0.001), decreasing in size distally. Note that the high maximum and minimum data values, illustrated by the whiskers, capture individual variation; however, the trend was the same across individuals.

To determine the relative CSA at each position along the rib, data were normalized by using the median position (50%) as the reference point. The proximal position on average was found to have a 22% greater CSA than the midpoint, while the distal position showed a 7% reduction (Fig. 4B). Based on these data the general shape of the rib is that of an elongated curved cone with a slow taper that becomes more apparent after 25% of the total length. Fig. 4C illustrates the general trend of the hollow cylinder at the three test points.

A structure's resistance to bending is determined not only by its stiffness (E) but also by the second moment of area. The second moment of area (I_{NA}) was found to decrease caudally for all individuals (quadratic regression; R^2=0.71; $F_{1,47}$=25.11; P<0.001);

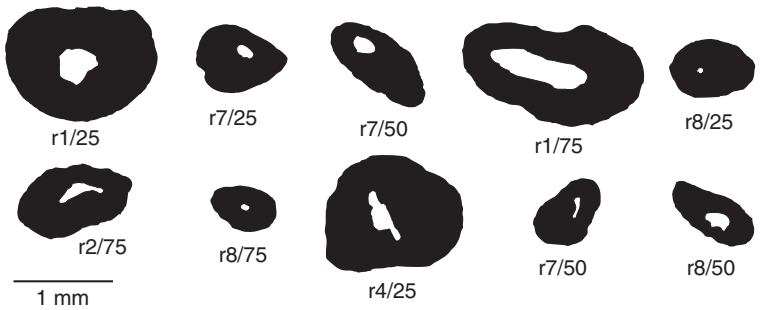

Fig. 2. Silhouette images from various individuals showing the morphological variation in the cross-sectional area (CSA) of both bone material and the hollow cylinder (shown in white) at one of three positions (25%, 50%, 75%) along the length of the rib. Note: r1/25=rib 1, 25% position.

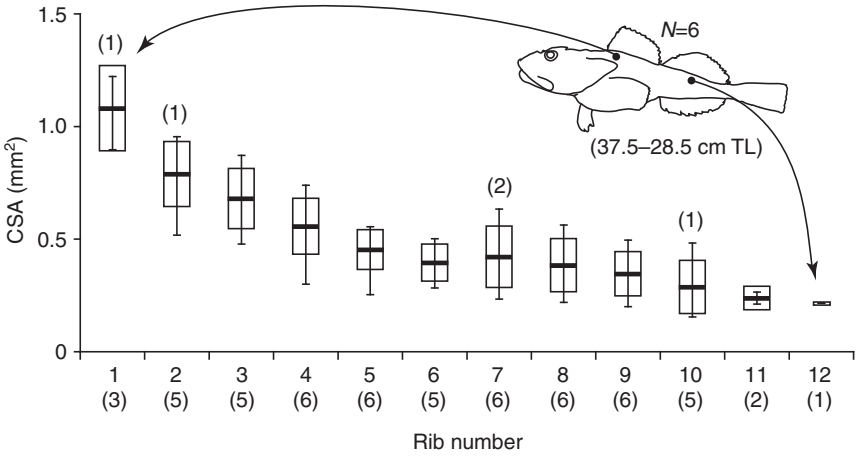

Fig. 3. Geometric CSA of the first to twelfth ribs of *M. polyacanthocephalus*. The CSA significantly decreased caudally for all individuals (quadratic regression; R^2=0.87; $F_{1,47}$=25.11; P<0.001). Individuals differed significantly due to the size variability but the overall trends were the same (P<0.001). A substantial difference was found in CSA between the first and second ribs, which was roughly 40%, and a relatively minor CSA difference between subsequent ribs of approximately 10%. The maximum CSA was 1.25 mm^2 at the first rib and 0.21 mm^2 at the twelfth rib. Values adjacent to the rib number on the *x*-axis correspond to the number of ribs tested. Numbers in parentheses above a data point indicate the total number of ribs containing a callus ring at some point along its structure. Arrows indicate relative position of the first and twelfth rib in the fish body. All data were pooled. Black bars denote the mean, the box represents the 95% confidence interval, and the whiskers are the maximum and minimum values of a given data point. TL, total length.

and, while individuals differed, the trends were the same (Fig. 5). Results were similar to the geometric, or first moment of area, data (see Fig. 3), including the considerable difference between the mean I_{NA} values of the first and second rib, of 48%, and subsequent ribs that differed by no more than 10% (Fig. 5). The maximum average I_{NA} was 0.12 mm^4 at the first rib and 0.01 mm^4 at the twelfth rib. Although individuals differed significantly (P<0.001), raw data from individuals exhibited a similar I_{NA} trend as shown in Fig. 5.

The mean I_{NA} was found to significantly decrease distally along the length of a rib for all individuals (R^2=0.87; $F_{2,10}$=5.99, P=0.016; Fig. 6A). The maximum and minimum data values indicated by the whiskers correspond to individual differences in I_{NA} for a given rib, as no size effect was found, and trends were the same across individuals. Furthermore, the absolute maximum I_{NA} was 0.252 mm^4 found at the 25% position and the absolute minimum was 0.001 mm^4 at the 75% position (see Fig. 6A). To determine the relative difference between I_{NA} at each of the three positions we normalized the data by using the midpoint position (50%) as the reference. The proximal position was found to be 56% greater than the midpoint, compared with the relatively small

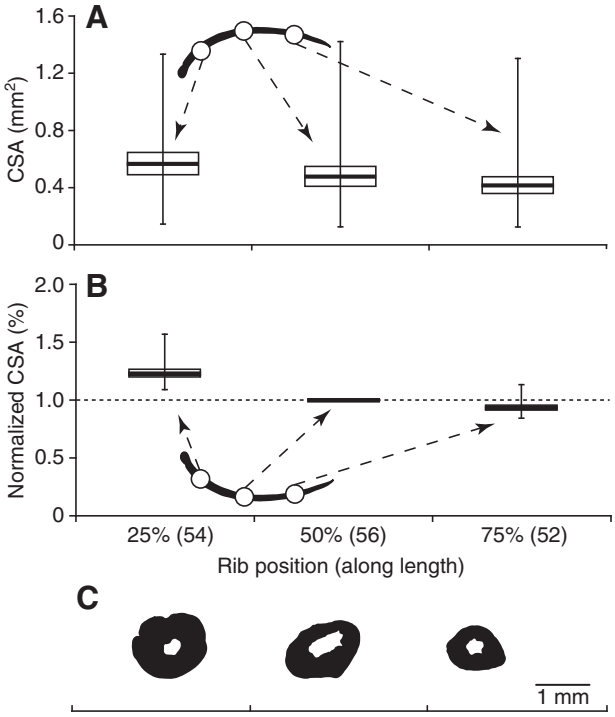

Fig. 4. The positional effect of the CSA along the length of a rib bone. (A) Variation in CSA along the length of the ribs at three locales (25%, 50%, 75%). The mean CSA decreased significantly distally for all individuals (R^2=0.95; $F_{2,10}$=25.11, P<0.001). Note that the high maximum and minimum data values, illustrated by the whiskers, correspond to individual differences; however, trends were the same across individuals. (B) Relative CSA at the three positions along the length of the rib referenced by the midpoint of the rib (50%), indicated by the dashed line. Compared with the midpoint the proximal position had a 21% greater area in contrast to a 7% reduction distally. All data were pooled. Black bars denote the mean, the box represents the 95% confidence interval, and the whiskers are the maximum and minimum values of a given data point. Values adjacent to rib position on the *x*-axis correspond to the total number of sections tested from a given locale. (C) Silhouettes of the CSA at three points along the length of a rib: 25%, 50% and 75%, from left to right.

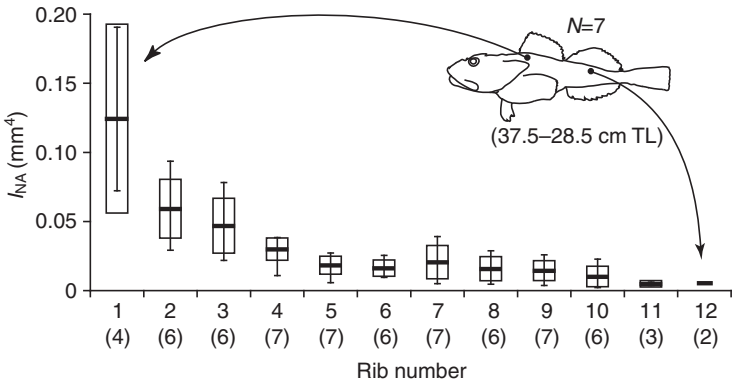

Fig. 5. Mean second moment of area (I_{NA}) of the first to twelfth ribs of *M. polyacanthocephalus*. I_{NA} was found to decrease significantly caudally for all individuals (quadratic regression; R^2=0.71; $F_{1,47}$=25.11; P<0.001). Individuals differed significantly due to the size variability but the overall trends were the same (P<0.001). A sizeable difference was found in I_{NA} values between the first and second ribs, which was approximately 48%, and a relatively minor difference between subsequent ribs of roughly 10%. The maximum I_{NA} was 0.12 mm^4 at the first rib and 0.01 mm^4 at the twelfth rib. Values adjacent to the rib number on the *x*-axis correspond to the number of ribs tested. Arrows indicate the relative position of the first and twelfth rib in the fish body. All data were pooled. Black bars denote the mean, the box represents the 95% confidence interval, and the whiskers are the maximum and minimum values of a given data point.

8% increase at the distal locale (Fig. 6B). The increased I_{NA} at the proximal position of the ribs is generally associated with the prominent hole typically found at this location.

The mean Young's modulus, or stiffness (E), of the acellular ribs ranged from 3.67 to 8.40 GPa with a mean ± s.e.m. of 6.48±0.31 GPa (Fig. 7A). A quadratic effect was found for all individuals (R^2=0.30; $F_{1,47}$=9.28, P<0.01; quadratic coefficient=–0.097), as rib stiffness increased to a peak value of 8.40 GPa at rib number 5 and then gradually decreased caudally. As expected, no significant linear effect was found (R^2=0.20; $F_{1,47}$=0.53; P=0.47); stiffness data did not exhibit the same trends as first and second moments of area (see Figs 3 and 5). No interaction was found between fish size and rib stiffness (P=0.22).

The material stiffness (E) was calculated at three points along the length of an individual rib. E decreased significantly distally at each of the three positions for all individuals ($F_{2,144}$=4.16; P=0.018), and the positional effect was consistent across ribs (Fig. 7B). E was highest at the proximal locale (25%) and presented a general downward trend distally; ribs 11 and 12 exhibited non-significant trends.

The flexural stiffness (EI), the product of the two primary factors that ultimately contribute to bending resistance of a structure, showed similar trends to the first and second moments of area but not to material stiffness (Fig. 8). The mean EI differed significantly between ribs (linear effect: R^2=0.79; $F_{1,48}$=134.86; P<0.001) and between position (linear effect: $F_{2,148}$=14.77; P<0.001). The geometric data permitted us to generate a moment ratio, which

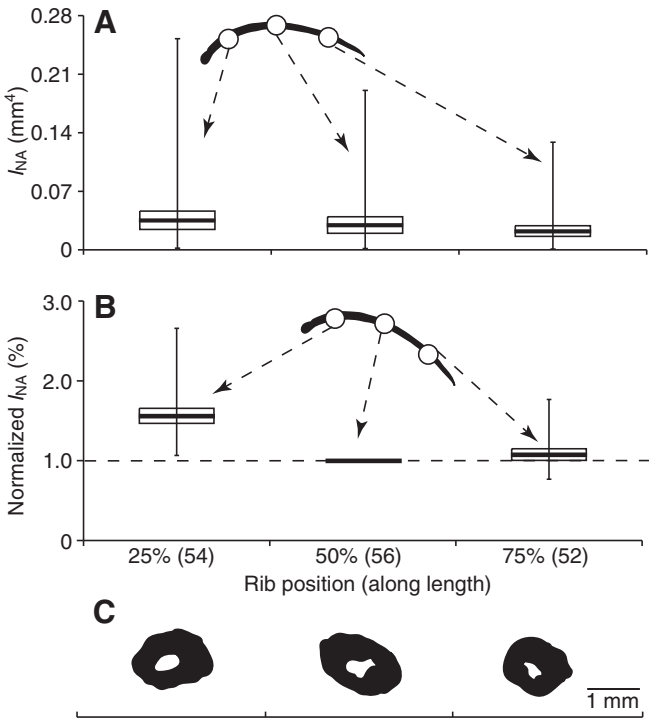

Fig. 6. Variation in I_{NA} along the length of the ribs at three relative positions (25%, 50% and 75%). (A) The mean I_{NA} significantly decreased distally for all individuals (R^2=0.87; $F_{2,10}$=5.99, P=0.02), and between positions. The maximum and minimum data values indicated by the whiskers correspond to individual differences in I_{NA} for a given rib, as no size effect was found (P>0.05) and trends were the same across individuals. The maximum I_{NA} was 0.252 mm^4 found at the 25% position and the minimum was 0.001 mm^4 at the 75% position. (B) Relative I_{NA} at three positions along the length of the rib referenced to the midpoint (50%). The proximal position was found to be 56% greater than the midpoint, compared with the 8% increase at the distal locale. The increased I_{NA} at the proximal position of the ribs is generally associated with the prominent hole typically found at this location. All data were pooled. Black bars denote the mean, the box represents the 95% confidence interval, and the whiskers are the maximum and minimum values of a given data point. Values adjacent to rib position on the *x*-axis correspond to the total number of sections tested from a given locale. (C) Silhouettes of the CSA at three points along the length of a rib: 25%, 50% and 75%, from left to right.

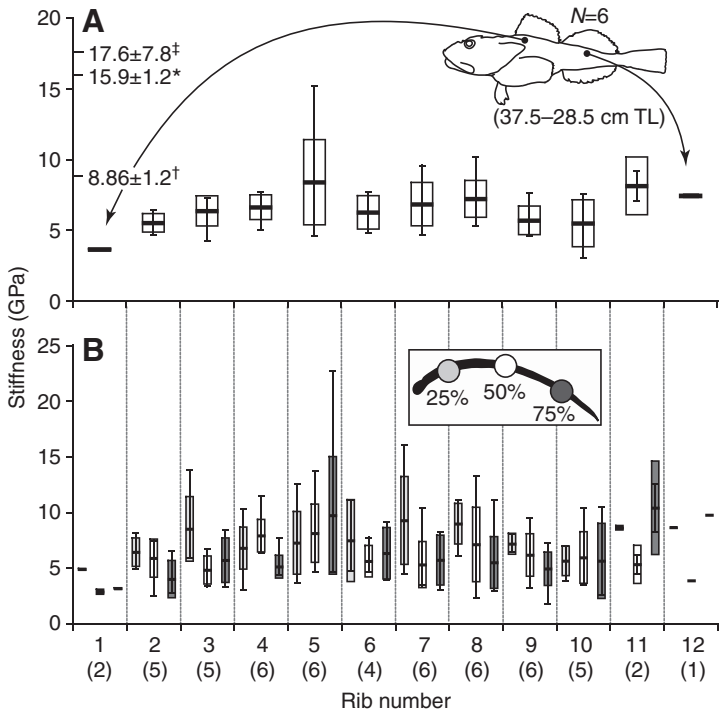

Fig. 7. (A) Mean Young's modulus (*E*) of the first 12 ribs from the cranial to caudal direction of *M. polyacanthocephalus*. The range fell between 3.67 and 8.40 GPa with a series mean ± s.e.m. of 6.48±0.31 GPa. A quadratic effect of rib stiffness was found for all individuals (R^2=0.30; $F_{1,47}$=9.28, P<0.01; quadratic coefficient=–0.097). The material stiffness increased to a peak value of 8.40 GPa at rib number 5 and then gradually decreased caudally. Comparison of material stiffness values of acellular bone in this study with those of cellular bone in other fishes are denoted by the symbols on the *y*-axis: carp (*Cyprinus carpio*) rib bone in a transverse plane (*) and longitudinal plane (†) tested by nanoindentation (Roy et al., 2000), and pelvic metapterygia (‡) of *Polypterus* sp. tested by three-point bending (Erickson et al., 2002). (B) Positional differences in material stiffness along the length of a rib; values are in sequential position order as indicated in the key. The stiffness decreased significantly distally at each of the three positions for all individuals ($F_{2,144}$=4.16; P=0.018); ribs number 11 and 12 exhibited non-significant trends. The three data points in a given column bounded by dashed lines correspond to, and are used to determine, mean elastic modulus of the same rib found above in A. Values adjacent to the rib number on the *x*-axis correspond to the number of ribs tested. Graphs contain pooled data; black bars are the mean, box represents the 95% confidence interval, and whiskers are the maximum and minimum values of the data.

showed that the hollow cylinder increases the flexural stiffness by 12.0% on average over a solid cylinder of similar external dimensions (Fig. 9). A value greater than 1 indicates that the rib structure with a hollow cylinder better resists bending, whereas a value less than 1 means a higher bending resistance for the solid cylinder; if equal, an indistinguishable difference in efficiency between the two structures would result.

Compositional analysis

There was no significant difference in the mineral content (% dry mass) between ribs (R^2=0.457; P=0.484). In addition, percentage mineral content did not differ between individuals ($F_{13,27}$=0.91; P=0.744; Fig. 10). Therefore, regardless of size or location, each rib contained the same amount of mineral – 71% of dry mass.

DISCUSSION

We have shown that the material stiffness of the acellular rib bone of the great sculpin (*Myoxocephalus polyacanthocephalus*) falls within the expected range for vertebrate cellular bone: 6.7–34.1 GPa (Currey, 1999). However, the mean stiffness (6.48 GPa) is lower than that reported for two species of fish with cellular bone: the ribs of *Cyprinus carpio* [8.1 GPa; using nano-indentation (Roy et al., 2000)] and the pelvic metapterygia of *Polypterus* sp. [17.6 GPa; using three-point bending (Erickson et al., 2002)]. This is contrary to our expectation that acellular bone would be stiffer because the solid material should be stiffer than material permeated with holes and channels.

The flexural stiffness of a structure, which is the product of *E* and *I*, is the measure of an object's ability to resist bending.

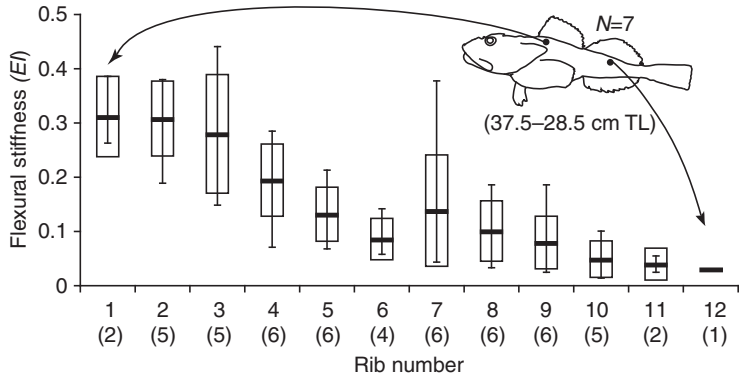

Fig. 8. Flexural stiffness (*EI*) of the first 12 ribs in the cranial to caudal direction of *M. polyacanthocephalus*. Data followed the same trend as first and second moments of area for ribs along the body. The mean *EI* differed significantly between ribs (linear effect: R^2=0.79; $F_{1,48}$=134.86; P<0.001), and between position (linear effect: $F_{2,148}$=14.77; P<0.001). The maximum mean value was 0.312, the minimum mean value was 0.031. Values adjacent to the rib number on the *x*-axis correspond to the number of ribs tested. Graphs contain pooled data; black bars are the mean, box represents the 95% confidence interval, and whiskers are the maximum and minimum values of the data.

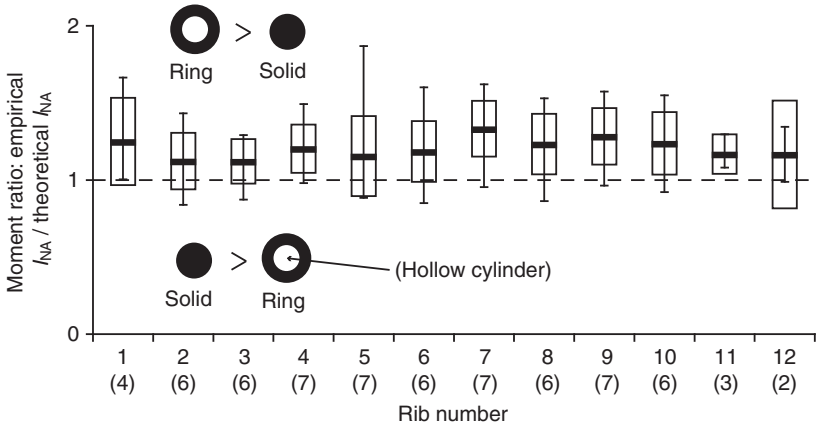

Fig. 9. Moment ratio: empirical *vs* theoretical second moment of area (I_t) for each rib. The contribution of the hollow cylinder morphology to flexural stiffness was calculated from the ratio of the measured I_{NA} of a rib to that of a solid cylinder with the same first moment of area as the rib section: $I_t=A_R^2/4\pi$; where A_R is the area of the rib cross-section. A value greater than 1 indicates that the rib structure with a hollow cylinder better resists bending, whereas a value less than 1 indicates that a solid cylinder better resists bending. A value of 1 – illustrated by the dashed line – indicates that the rib is just as good at resisting flexion as a solid cylinder. Values adjacent to the rib number on the *x*-axis correspond to the number of ribs analyzed. Graph contains pooled data; black bars are the mean, box represents the 95% confidence interval, and whiskers are the maximum and minimum values of the data.

Variation in the ability of sculpin ribs to resist bending is primarily due to the geometric arrangement (I_{NA}) rather than stiffness (E) of the bone, as the flexural stiffness of the ribs along the body correlates with both first and second moments of area (Fig. 8) but not with material stiffness or mineral content (Figs 7 and 10). Our data show a range difference of almost 3 times for the elastic modulus, and approximately 13 times in second moment of area (Figs 5 and 6). It can therefore be concluded that the structural arrangement of the material (including mineral distribution) accounts for either the decrease or increase in stiffness, as seen across the rib series and along a rib. We conclude that structure dominates, assuming uniform mineral distribution, and is the primary determinant of variation in flexural stiffness.

The ribs of the great sculpin are hollow cylinders of bone (Fig. 2), though neither of the usual explanations for this morphology are likely causal factors in this fish. In tetrapods, but not teleost fishes, the hollow bone marrow cavity contains hematopoietic and mesenchymal stem cells (Liem et al., 2000). A second function of hollow bones is mechanical: hollow cylinders have an increased second moment of area (I) relative to solid cylinders of the same mass. Both flexural stiffness (EI) and Euler buckling [$F=(K\pi^2EI)/l^2$] are dependent on I, so a stiffer and less failure-prone bone can be constructed of less material if it is hollow. One structure that takes advantage of the added strength is the hollow tubes in the jaws of the durophagous horn shark, *Heterodontus francisci*, which are 60 times stiffer due to their shape (Summers et al., 2004), allowing the organism to resist jaw deformation while crushing hard prey. Our results have shown that while there is a small increase in flexural stiffness due to the hollow cavity in ribs (Fig. 9) the advantage is not nearly as great as that seen in mammals and birds (Biewener, 1982), or cartilaginous fishes (Summers et al., 2004). We suppose that the ribs of teleost fishes are hollow for other reasons. The hollow core may increase the surface area for bone resorption as it has been suggested that acellular bone is mobilized for calcium homeostasis during calcium deficiency (Takagi and Yamada, 1992). Also, tubular structures are most efficient in dealing with multidirectional loading or torsional stress (Currey, 2003), which are the likely loading conditions of the ribs given their anatomical position;

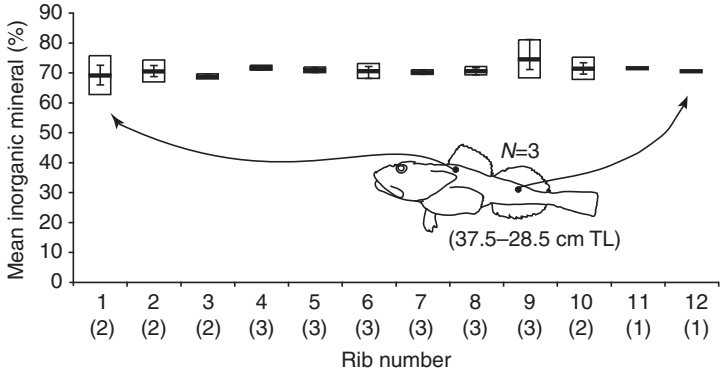

Fig. 10. Mean mineral content (% dry mass) of the first to twelfth ribs of *M. polyacanthocephalus*. All ribs were found to contain the same percentage mineral material, as no significant difference was found between ribs (R^2=0.457; P=0.484) or individuals ($F_{13,27}$=0.91; P=0.744). The mean percentage mineral was 70.89% dry mass. Values adjacent to the rib number on the *x*-axis correspond to the number of ribs analyzed at a give locale. Arrows indicate the relative position of the first and twelfth rib in the fish body. All data were pooled. Black bars denote the mean, the box represents the 95% confidence interval, and the whiskers are the maximum and minimum values of a given data point.

therefore the ribs may be hollow to resist structural failure when they are subjected to multiple loading regimes.

Although bone stiffness does not appear to explain the adaptive significance of acellular bone, their acellularity may have a beneficial effect on other material properties. Low stiffness values are normally correlated with decreased mineral levels. However, a decrease in mineral content may lead to a more compliant material better equipped to resist fatigue damage, whereas porous materials are typically better at limiting crack propagation. Future work on strength, toughness and fatigue resistance may reveal possible selective pressures that explain the multiple evolutions and recent prevalence of acellularity in teleost fishes.

We would like to thank the UC Irvine Biomechanics group for their thoughtful comments and suggestions on this manuscript, and all those who supported J.M.H. throughout the process, especially Maria Virginia Sanchez-Puerta, and Diane Campbell for statistical assistance. A special thank you to Friday Harbor Laboratories for their gracious hospitality, and for use of their facilities. This research was funded by National Science Foundation grant (IOB-0616322) to A.P.S.

REFERENCES

Aarden, E. M., Burger, E. H. and Nijweide, P. J. (1994). Function of osteocytes in bone. *J. Cell. Biochem.* **55**, 287-299.
Biewener, A. A. (1982). Bone strength in small mammals and bipedal birds: do safety factors change with body size? *J. Exp. Biol.* **98**, 289-301.
Burger, E. H. and Klein-Nulend, J. (1999). Mechanotransduction in bone-role of the lacuno-canalicular network. *FASEB J.* **13**, S101-S112.
Burr, D. B., Robling, A. G. and Turner, C. H. (2002). Effects of biomechanical stress on bones in animals. *Bone* **30**, 781-786.
Cowin, S. C. (2007). The significance of bone microstructure in mechanotransduction. *J. Biomech.* **40**, S105-S109.
Currey, J. D. (1999). The design of mineralized hard tissues for their mechanical functions. *J. Exp. Biol.* **202**, 3285-3294.
Currey, J. D. (2002). *Bones: Structure and Mechanics*. Princeton, NJ: Princeton University Press.
Donahue, H. J. (2000). Gap junctions and biophysical regulation of bone cell differentiation. *Bone* **26**, 417-422.
Erickson, G. M., Catanese, J. and Keaveny, T. M. (2002). Evolution of the biomechanical material properties of the femur. *Anat. Rec.* **268**, 115-124.
Fratzl, P. and Weinkamer, R. (2007). Nature's hierarchical materials. *Prog. Mater. Sci.* **52**, 1263-1334.
Gray, D. J. (1941). Length of lacunae and number of canaliculi in bones of several mammals. *Anat. Rec.* **81**, 163-169.
Hanken, J. and Hall, B. K. (1993). *The Skull: Patterns of Structural and Systematic Diversity*. Chicago, IL: University of Chicago Press.
Kölliker, A. (1859). On the different types in the microscopic structure of the skeleton of osseous fish. *Proc. Biol. Sci.* **9**, 656-688.
Kranenbarg, S., van Cleynenbreugel, T., Schipper, H. and van Leeuwen, J. (2005a). Adaptive bone formation in acellular vertebrae of sea bass (Dicentrarchus labrax L.). *J. Exp. Biol.* **208**, 3493-3502.
Kranenbarg, S., Waarsing, J. H., Muller, M., Weinans, H. and van Leeuwen, J. L. (2005b). Adaptive bone formation in acellular vertebrae of sea bass (Dicentrarchus labrax L.). *J. Biomech.* **38**, 1239-1246.
Kusuzaki, K., Kageyama, N., Shinjo, H., Takeshita, H., Murata, H., Hashiguchi, S., Ashihara, T. and Hirasawa, Y. (2000). Development of bone canaliculi during bone repair. *Bone* **27**, 655-659.
Lanyon, L. E. (1993). Osteocytes, strain detection, bone modeling and remodeling. *Calcif. Tiss. Int.* **53 Suppl.** 1, S102-S106; discussion S106-S107.
Liem, K. F., Bemis, W., Walker, W. F. and Grande, L. (2000). *Functional Anatomy of the Vertebrates: An Evolutionary Perspective*. Fort Worth, TX: Brooks Cole.
Meunier, F. J., Sorba, L. and Béarez, P. (2003). Presence of vascularized acellular bone in the elasmiod scales of *Micropogonias altipinnis* (Osteichthyes, Perciformes, Sciaenida). *Cybium* **28**, 25-31.
Meunier, F. J., Sorba, L. and Béarez, P. (2004). Presence of vascularized acellular bone in the elasmoid scales of *Micropogonias altipinnis* (Osteichthyes, Perciformes, Sciaenidae). *Cybium* **28**, 25-31.
Mjor, I. A. (1962). Bone matrix adjacent to lacunae and canaliculi. *Anat. Rec.* **144**, 327-339.
Moss, M. L. (1960). Osteogenesis and repair of acellular teleost bone. *Anat. Rec.* **136**, 246-247.
Moss, M. L. (1961). Osteogenesis of acellular teleost fish bone. *Am. J. Anat.* **108**, 99-109.
Moss, M. L. (1962). Studies of acellular bone of teleost fish. 2. Response to fracture under normal and acalcemic conditions. *Acta Anat.* **48**, 46-60.
Moss, M. L. (1965). Studies of acellular bone of teleost fish. 5. Histology and mineral homeostasis of fresh-water species. *Acta. Anat.* **60**, 262-276.
Moss, M. L. and Freilich, M. (1963). Studies of acellular bone of teleost fish. 4. Inorganic content of calcified tissues. *Acta Anat.* **55**, 1-8.
Mullender, M. G., Huiskes, R., Versleyen, H. and Buma, P. (1996). Osteocyte density and histomorphometric parameters in cancellous bone of the proximal femur in five mammalian species. *J. Orthop. Res.* **14**, 972-979.
Ørvig, T. (1965). Paleohistological notes. 2. Certain comments on the phyletic significance of acellular bone tissue in early lower vertebrates. *Ark. Zool.* **16**, 551-556.
Ørvig, T. (1989). Histologic studies of ostracoderms, placodermes, and fossil elasmobranches. 6. Hard tissues of Ordovician verebrates. *Zool. Scr.* **18**, 427-446.
Roy, M. E., Nishimoto, S. K., Rho, J. Y., Bhattacharya, S. K., Lin, J. S. and Pharr, G. M. (2000). Correlations between osteocalcin content, degree of mineralization, and mechanical properties of C. Carpio rib bone. *J. Biomed. Mater. Res.* **54**, 547-553.
Sansom, I. J., Smith, M. P., Armstrong, H. A. and Smith, M. M. (1992). Presence of the earliest vertebrate hard tissue in conodonts. *Science* **256**, 1308-1311.
Schaffler, M. B. and Burr, D. B. (1988). Stiffness of compact-bone-effects of porosity and density. *J. Biomech.* **21**, 13-16.
Spatz, H. C., O'Leary, E. J. and Vincent, J. F. V. (1996). Young's moduli and shear moduli in cortical bone. *Proc. Biol. Sci.* **263**, 287-294.
Summers, A. P., Ketcham, R. A. and Rowe, T. (2004). Structure and function of the horn shark (Heterodontus francisci) cranium through ontogeny: development of a hard prey specialist. *J. Morphol.* **260**, 1-12.
Takagi, Y. and Yamada, J. (1992). Effects of calcium deprivation on the metabolism of acellular bone in Tilapia, Oreochromis-niloticus. *Comp. Biochem. Physiol. A* **102**, 481-485.
Takagi, Y. and Yamada, J. (1993). Changes in metabolism of acellular bone in Tilapia, Oreochromis-niloticus, during deficiency and subsequent repletion of calcium. *Comp. Biochem. Physiol. A* **105**, 459-462.
Wassermann, F. and Yaeger, J. A. (1965). Fine structure of the osteocyte capsule and of the wall of the lacunae in bone. *Z. Zellforsch.* **67**, 636-652.
Young, W. C. and Budynas, R. G. (2002). *Roark's Formulas for Stress and Strain*. 7th edn. New York: McGraw-Hill.